



or treatment options [8], [9]. Meanwhile, it has been observed that the overuse of diagnostic imaging is on the rise in clinical practices causing a significant stress on health budget and fundings [10]. As a result, current guidelines emphasize the importance of using risk stratification tools and pre-test probability assessment tools (i.e., to assess the likelihood of disease) prior to initiation of downstream testing. However, their lack of general applicability has been identified as a limitation. Multiple studies have shown that these risk assessment models perform sub-optimally in certain groups of patients [5], [11]. Patients have varying underlying conditions that require personalized approach. Furthermore, differences in derivation (variations in the way these models are developed, such as the use of different imaging modalities, cut-off values for defining CAD risk, and data processing techniques) often occur and may further limit the effectiveness of these tools. Machine learning models are ideally suited for addressing these challenges. It could suggest an optimized probability based on the most recent locally relevant data as input. Therefore, our aim was to develop a machine learning model, using the CCTA diagnostic test reports of patients as input. These data are collected as tabular data.

As a subfield of machine learning, deep neural networks has achieved dazzling success in a wide variety of areas, such as computer vision and natural language processing using transformer-based architecture [12], [13]. For tabular data, tree-based machine learning or ensemble models are reported as the best algorithms [14]–[16], as these models have been found to be effective in delivering good performance with less training time and are easily explainable. However, tree-based models can be sensitive to small changes in the input and have limitations when dealing with limited labeled data when advanced semi-supervised learning techniques are used and in handling high dimensional data [17], [18]. Conversely, deep learning models have their own strengths, such as the ability to handle both single-task and multi-task learning of image or text inputs, or multi-modal input, including tabular data [19]. In this paper, we sought to apply deep learning to construct a multi-task learning model on tabular data.

It is logical to assume that the downstream diagnosis of each patient is primarily based on their CAD risk, so it makes a very strong case to consider the CAD risk and downstream diagnosis together. In this scenario, multi-task learning [20] is a viable solution as it allows to exploit useful information from these two related learning tasks.

Multitask learning, which is a promising field in deep learning, aims to improve the accuracy of learning each task by leveraging the useful information shared across multiple tasks. It has been empirically and theoretically demonstrated that learning multiple tasks can result in better performance than learning them individually [21]. In this research, we aimed to introduce a multi-task deep learning model for identifying patients who may benefit from invasive coronary investigation and revascularization. Our multi-task deep learning model was designed to learn from patient demographics, clinical history, and CCTA test readings, in order to predict patients' risk of CAD and their down-streaming investigations and treatment options.

The contributions of this paper are summarized as following:

- The introduction of TabPerceiver, a simple and less computationally expensive transformer-based deep learning model that can handle multi-modal data.
- The multi-task TabPerceiver model automatically associates downstream diagnosis and treatment with patient CAD risk.
- Demonstrating that TabPerceiver achieved better performance than gradient boosting decision trees but there is no universally superior solution between GBDT and deep learning models for tabular data.

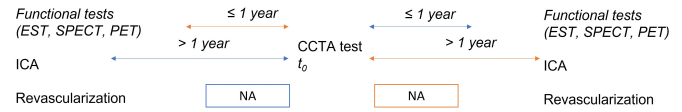


Fig. 2. Timeline of cohort selection and output definition. We identified patients who had CCTA, and  $t_0$  is the date of their index CCTA. Patients who have undergone previous tests or treatments within 1 year before  $t_0$  are excluded. The eligible down-streaming tests should be conducted within 1 year after  $t_0$ . Patients with no follow-up records are excluded since their outcomes are unknown.

## II. METHODS

### A. Study Data

We used a substantial dataset acquired from the University of Ottawa Heart Institute, Canada. In the total cohort, 20,683 CCTA test reports were identified in the period between 2006 to 2017. The date of their first CCTA test was defined as  $t_0$ . The timeline is presented in Fig. 2. We excluded patients whose tests were cancelled or whose CCTA readings were missing. Additionally, we excluded duplicate reports for the same patients and kept records from experienced senior readers. Our cohort was further restricted to include patients who had CCTA as their primary test, and had not undergone revascularization or other tests (ICA, SPECT, PET, EST) within 1 year before  $t_0$ . More specifically, we included patients with i) CCTA as their initial test, ii) underwent at least one of the SPECT, PET, EST, ICA or revascularizations (percutaneous coronary intervention (PCI) and coronary artery bypass graft surgery (CABG)) within one year after  $t_0$ , and iii) had a second test interpretation available. This resulted in the selection of a cohort of 884 patients as showed in Fig. 3. All reported results were obtained from a held-out test set that was not used to train or tune the model.

### B. Predictors

Each patient entry included demographic information (age, sex, weight, and height), clinical information (heart rate, blood pressure, and reasons for test), pretest probability of CAD (Diamond & Forrester) [22], significant cardiovascular risk factors (family history, smoking status, diabetes mellitus, hypertension, hyperlipidemia, and history of CAD), medications (aspirin, beta-blockers, calcium channel blockers, statins, and metformin) and CCTA segment stenosis readings. All of this information was included as input to our models.

### C. Pre-processing

We removed features that had more than 50% missing values and imputed the remaining missing values in 22 features with maximum missing rate of 8.8% using multivariate imputation [23]. All the other

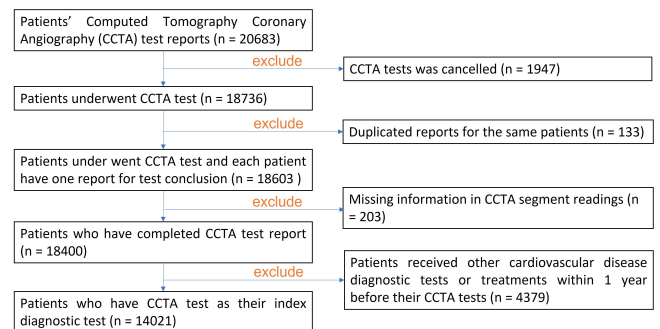


Fig. 3. Cohort selection based on patients' CCTA test report availability and investigation journey.





input features were used to estimate the missing values in a round-robin fashion.

#### D. Outcomes

We linked the diagnostic tests and revascularization data for each individual patient using the available data. The downstream tests or treatments were those performed within one year after their CCTA tests. We separated the downstream test or treatments into two groups: functional testing (including EST, SPECT and PET) vs. invasive tests and/or revascularization (including ICA, PCI and CABG). This makes the downstream tests or treatments prediction to be a binary classification task.

The risk of CAD for patients was determined by the readings of the follow-up tests as shown in Fig. 4. The risk of patients was classified into three groups: low, intermediate and high risk. Then the risk prediction task becomes a classification task with multiple classes. Based on the tests and data availability, the risks of CAD were defined differently for each test.

The results of the test were used to determine the risk for patients who had EST after their CCTA. The Summed Difference Score (SDS) was used to determine the risk of CAD for patients who received SPECT and PET [24]. This was determined by test findings for patients who had ICA. Patients who were scheduled for revascularisation were determined to be at high risk.

<b>Functional testing</b>		<b>SDS &lt; 2, or normal in predefined fields*</b>
SPECT 	<b>2 ≤ SDS ≤ 6, or 1 abnormal in predefined fields*</b>	
	<b>SDS &gt; 6, or ≥2 abnormal in predefined fields*</b>	
	<b>SDS &lt; 2</b>	
PET 	<b>2 ≤ SDS ≤ 6</b>	
	<b>SDS &gt; 6</b>	
	<b>Negative EST</b>	
EST 	<b>Positive EST</b>	
	<b>Strong positive EST</b>	
	<b>Normal anatomy</b>	
ICA / Revascularization 	<b>Non-significant CAD</b>	
	<b>Revascularization (PCI, CABG)</b>	
	<b>Invasive</b>	

■ low risk  
■ intermediate risk  
■ high risk

**Fig. 4.** Output labeling. The test conclusions were utilised to determine the risk of CAD for patients who had EST following their CCTA. The Summed Difference Score (SDS) was used to determine the risk of CAD for patients who received SPECT and PET. [24] This was determined by test findings for patients who had ICA. Patients who were assigned for revascularisation were determined to be high risks. Predefined fields included: scar, ischemia, LAD, RCA, LCX, RCALCX, TID, DilatedLV. LAD, left anterior descending artery; RCA, right coronary artery; LCX, left circumflex artery; TID, transient ischemic dilation; LV, left ventricular; ICA, invasive coronary angiography; PCI, percutaneous coronary intervention; CABG, coronary artery bypass graft surgery

#### E. Statistical analysis and metrics for performance measure

The discriminant power of the risk prediction and downstream test or treatment recommendation tasks was evaluated using the area under the receiver operating characteristic curve (AU-ROC) with a 95% confidence interval (CI). We also reported sensitivity (recall), specificity, precision (positive predictive value) and negative predictive value. The calibration was evaluated using the Brier score, which calculates the difference between the estimated and observed

results. We evaluated the performance of GBDT, multi-layer perceptron (MLP) and TabPerceiver in performing single task learning, and also assessed the performance of the multi-task TabPerceiver. We then compared the performance of different models using a paired sample T-test and reported the corresponding p-value. The group difference was compared using the chi-square test for categorical variables. One-way ANOVA was used to compare the means of continuous variables across distinct risk groups, whereas the T-test was used to compare downstream diagnostic tests or treatments. We regarded the performance difference to be statistically significant if there was no overlap between 95% CIs and the p-value was less than 0.05.

#### F. The architecture of TabPerceiver

We have extended the architecture of Perceiver-IO [25] and Tab-transformer [26] to create the Tab-Perceiver. Perceiver-IO is an advanced artificial intelligence architecture that can handle arbitrary inputs and outputs. It can produce various outputs, such as language and video, and is built on the same building blocks as the original Perceiver [27]. It is computationally efficient and can handle large inputs and outputs than the standard self-attention Transformer [28]. We constructed separate embeddings for categorical and continuous features implementing different algorithms. The categorical and continuous embeddings were then fed into perceiver encoders individually. Perceiver encoder is a stack of cross-attention modules that transfer the input embedding to a latent vector, with a latent Transformer [29] converting one latent vector to another latent vector. The latent transformer consists of a multi-head self-attention layer. The perceiver decoder is constructed in a similar manner to the encoder. Both encoder and decoder take in two inputs. The first input is used as the input to the key and value network of the cross-attention module, while the second is used as the input to the query network. The architecture of TabPerceiver is shown in Fig. 5.

Let  $(x, y)$  denote a feature-target pair, where  $x \equiv \{x_{cat}, x_{num}\}$ .  $x_{num} \in \mathbb{R}^C$  denotes all of the  $C$  continuous features. Let  $x_{cat} \equiv \{x_1, x_2, \dots, x_M\}$  with each  $x_i$  being a categorical feature, for  $i \in \{1, \dots, M\}$ . We embedded each of the  $x_i$  categorical features into a parametric embedding of dimension  $D$  using feed-forward network with a learnable embedding layer. Let  $e_{\phi_i}(x_i) \in \mathbb{R}^D$  for  $i \in \{1, \dots, M\}$  be the embedding of the  $x_i$  feature, and  $E_{\phi}(x_{cat}) = \{e_{\phi_1}(x_1), \dots, e_{\phi_M}(x_M)\}$  be the set of embeddings for all the categorical features.

Next, these parametric embeddings  $E_{\phi}(x_{cat})$  are input to the perceiver encoder. The perceiver encoder alternatively employed the cross-attention and the Transformer (self-attention) modules. Both cross-attention and self-attention modules are organised around the use of query-key-value (QKV) attention. QKV attention applies three networks - the query, key, and value networks, which are typically MLPs. To each element of  $E_{\phi_i}(x_{cat})$ , producing three vectors that preserve the index dimensionality  $M$ .

To understand how this works in self-attention, it is important to first note that for  $Q \in \mathbb{R}^{M \times D}$ ,  $K \in \mathbb{R}^{M \times D}$ , and  $V \in \mathbb{R}^{M \times D}$ , (where  $D$  is the dimension of embedding) the complexity of the QKV attention operation - essentially,  $\text{softmax}(QK^T)V$  - is  $\mathcal{O}(M^2)$ , as it involves two matrix multiplications with matrices of dimension  $M$ . In cross-attention, while  $K$  and  $V$  are projections of the input,  $Q$  is a projection of a learned latent array with index dimension  $N$ , where the latent's dimension  $N$  is a hyper-parameter. Consequently, the cross-attention operation has complexity  $\mathcal{O}(MN)$ .

The output of the cross-attention module takes the shape of the  $e_{\phi_i}(x_i)$  to the  $Q$  network. Hence, the cross-attention layer introduces a bottleneck. We can then further analyze this bottleneck in depth by utilizing multi-head self-attention module in the latent space, and

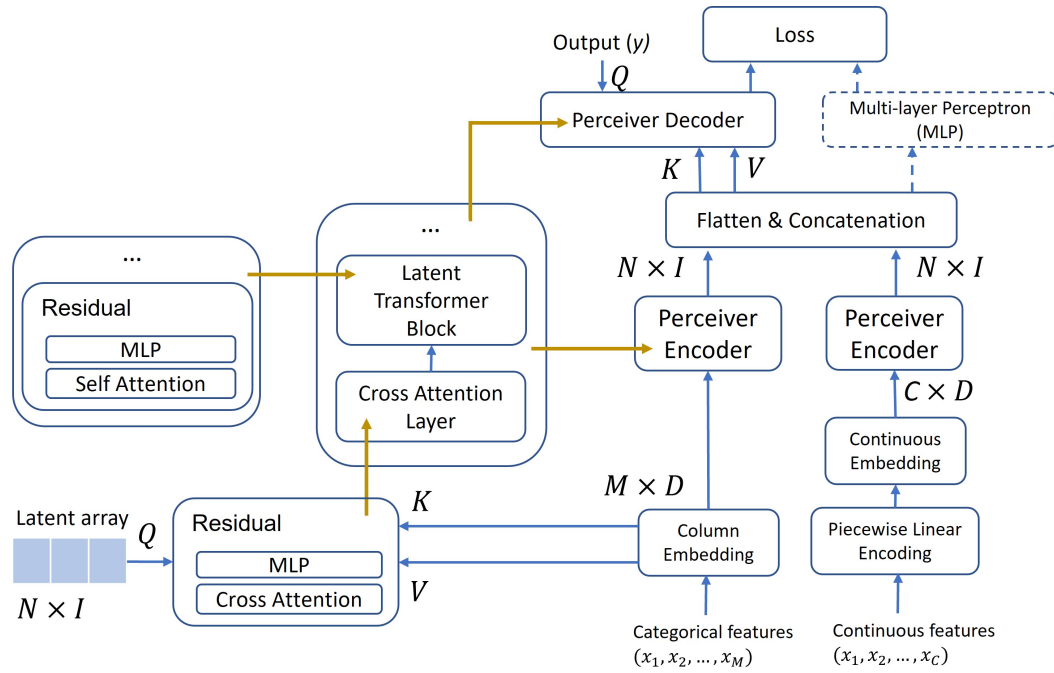


**Fig. 5.** The TabPerceiver architecture. It uses a cross-attention module to project the input embeddings to a fixed-dimensional latent bottleneck and then processing it using a stack of Transformer-style self-attention blocks in the latent space. The latent indices  $N$  and latent dimension  $I$  are hyper-parameters and independent from the number of input features  $M$  and  $C$ .  $D$  is the dimension of embedding. The encoder iteratively attends to the input by alternating cross-attention and latent self-attention blocks. The decoder takes the concatenated output of encoder as input to its query ( $K$ ) and value ( $V$ ) networks, and the model output was the input to its query ( $Q$ ) network.

the this comes at the cost of  $\mathcal{O}(N^2)$ . This results in an architecture with complexity  $\mathcal{O}(MN + LN^2)$ , where  $L$  represents the number of layers of self-attention module in perceiver encoder. The introduction of  $N$  decouples the input size from the depth of self-attention module, allowing for more flexibility in terms of the input size and depth of the model. For large-scale data with high dimension  $M$ ,  $N \ll M$ , helps to reduce the complexity of the model. This allows for construction of deep networks with a lower cost.  $N > M$  is also acceptable for small-scale tabular data with selected input features. It contributes to the expansion of input for subsequent layers.

The bottleneck may impede the network's ability to acquire detailed information from the input. To mitigate this impact, the perceiver encoder could be structured with multiple cross-attend layers that enable the latent vector to extract information from the input in an iterative manner, which helps to gather more detailed information from the input. Given that there is no ordering of the categorical features in tabular data, positional encoding is not applied. We denote the sequence of cross-attend layers as a function  $f_\theta$ . The function  $f_\theta$  operates on parametric categorical embeddings  $\{e_{\phi_1}(x_1), \dots, e_{\phi_M}(x_M)\}$  and returns the corresponding latent vector with shape  $N \times I$ , where the latent's channel  $I$  is another hyper-parameter.

Concurrently, continuous features were first encoded using piecewise linear encoding [30]. Let  $x_{num} \equiv \{x_1, x_2, \dots, x_C\}$  with each  $x_j$  being a continuous feature, for  $j \in \{1, \dots, C\}$ . For each  $x_j$ , we split its value range into the disjoint set of  $T$  bins according to their empirical quantiles, denoted as  $B_1, \dots, B_T$ .

$$B_t = [b_{t-1}, b_t), \quad (1)$$

where  $b_t$  is calculated using the empirical quantile function. Trivial bins of zero size are removed. Then we allocated one trainable embedding  $e_t$  for each bin  $B_t$  and aggregated the embeddings of its bins with  $v_t$  as weights, plus bias  $v_0$ . The embedding for each

continuous feature  $x_j$  can thus be denoted as:

$$e_t = \begin{cases} 0, & x < b_{t_1}, t > 1 \\ 1, & x \geq b_t, t < T \\ \frac{x - b_{t-1}}{b_t - b_{t-1}}, & \text{otherwise} \end{cases}, \quad (2)$$

$$e_{\varphi_j}(x_j) = v_0 + \sum_{t=1}^T e_t \cdot v_t, \quad (3)$$

and where  $E_\varphi(x_{cont}) = \{e_{\varphi_1}(x_1), \dots, e_{\varphi_C}(x_C)\}$  is the set of embeddings for all the continuous features. The latent vector of categorical features are then flattened and concatenated with the latent vector of continuous features to form a vector of dimension  $2NI$ . This vector is one of the input to perceiver decoder. We denote the decoder as a function  $g$ , and it also operates on the target  $y$ . Let  $H$  be the cross-entropy for classification tasks. We minimize the following loss function  $\mathcal{L}(x, y)$  to learn all the TabPerceiver parameters. The TabPerceiver parameters include  $\phi$  for column embedding,  $\theta$  for cross-attend layers.

$$\mathcal{L}(x, y) \equiv H(g(f_\theta(E_\phi(x_{cat})), f_\theta(E_\varphi(x_{num}))), y). \quad (4)$$

As an alternative to decoder, we investigated the use of MLP in the architecture. After undergoing embedding and perceiver encoder, the concatenated latent output of categorical and continuous embeddings can simply be passed through an MLP denoted as  $k_\psi$  to predict the target  $y$ . The equation (4) can be updated as below, if the MLP with  $\psi$  for the top layer were used after the encoder.

$$\mathcal{L}(x, y) \equiv H(k_\psi(f_\theta(E_\phi(x_{cat})), f_\theta(E_\varphi(x_{num}))), y). \quad (5)$$

Hard and soft parameter sharing are two prevalent techniques for performing multitask learning in deep neural networks. Hard parameter sharing maintains task-specific output layers while sharing the hidden layers between all tasks. Soft parameter sharing preserves

individual hidden layers for each task. [31] In our multitask TabPerceiver, we opted for the hard parameter sharing strategy, where we shared the hidden layers between all tasks, but kept task-specific output layers. We had two tasks during the learning, risk and downstream tests or treatments prediction, denoted  $y^t \in \mathbb{R}^N, t \in \{1, 2\}$ . We employed one decoder for each task, and then we applied uncertainty to weight the loss [32], where the weight  $w_i$  for each task is a learnable parameter. Then the equation for multi-task TabPerceiver would form as:

$$\mathcal{L}(x, y) \equiv \sum_{i=1}^T w_i \mathcal{L}(x, y^i). \quad (6)$$

### G. Feature selection

Feature ranking in GBDT was obtained by computing Shapley Additive Explanation values (SHAP) [33]. We then selected the top ranked features and fitted them in the GBDT. We conducted an ablation study to assess the importance of different features in TabPerceiver (demographics, clinical information, comorbidity history, medications, CCTA scan readings) by alternatively removing each of these features. We also experimented with the selected features in GBDT on the TabPerceiver model. The detailed feature and their selection results can be found in Appendix section "List of available and selected features".

### H. Hyper-parameter tuning

Bayesian optimization [34] was used to tune the model hyper-parameters for all the experimental models, including learning rates, batch size, bins count for continuous feature encoding, number of heads, cross-attend layers and latent dimension in TabPerceiver. We also tuned the number of estimators, number of leaves, maximum depth, minimum data in each leaf, maximum bin and subsample in GBDT. All the models were tuned on the validation set, and the optimal hyper-parameter setting for ML-TabPerceiver is listed in the Appendix section "Model hyper-parameters".

## III. RESULTS

### A. Patient characteristic

Out of the 894 patients in the cohort, 475 (53.7%) were determined to be high risk, 225 (25.5%) were found to be low risk, and around one-fifth of the patients, 184 (20.8%), were defined as intermediate risk. Of the total number of patients, 239 (27%) received functional testing as a downstream diagnostic test, while the remaining 645 (73%) received invasive testing or revascularization. The mean age was 59.0 years (SD 10.8) and 65.6% were male (Table I). Both hyperlipidemia (61.8%) and hypertension (56.3%) were prominent risk factors, whilst diabetes mellitus was presented in 16.2% of the population and 16.9% were current smokers. The mean baseline heart rate was 67 (SD 11.9), mean Agatston score was 361.3 (SD 551.4), and the mean baseline systolic and diastolic blood pressure were 137 (SD 19.7) and 79 (SD 10.4), respectively. As showed in Fig. 6, the CAD risks of patients are highly correlated with their down-streaming tests. Most of patients at high risks of CAD had invasive tests or treatments after their CCTA.

### B. Model performance using the selected features

Table II shows the AUC, sensitivity, specificity and brier score of the multi-task TabPerceiver with decoder using the selected input variables comparing the performance of single-task GBDT, MLP and TabPerceiver. GBDT outperformed the competitors while doing the single task learning. However, multi-task TabPerceiver showed the

TABLE I  
PATIENT CHARACTERISTICS

Patient characteristics	n(%) unless otherwise specified	p-value (CAD risk)	p-value (downstream tests)
Age, mean (SD), years	59.0 (10.8)	< 0.05	< 0.05
Male	580 (65.6)	0.49	0.32
Height (cm), mean (SD)	170.0 (10.5)	0.98	0.14
Weight (kg), mean (SD)	85.3 (18.4)	0.66	0.45
Baseline HR (bpm), mean (SD)	67 (11.9)	< 0.05	0.08
Baseline Systolic BP (mmHg), mean (SD)	137.0 (19.7)	0.07	0.41
Baseline Diastolic BP (mmHg), mean (SD)	79 (10.4)	0.34	0.52
Agatston, mean (SD)	361.3 (551.4)	< 0.05	< 0.05
Probability of CAD, mean (SD)	35.6 (31.2)	< 0.05	< 0.05
Family history of CAD	450 (50.9)	0.38	0.29
Hypertension	498 (56.3)	< 0.05	< 0.05
Hyperlipidemia	546 (61.8)	0.37	0.10
Diabetes mellitus	143 (16.2)	< 0.05	0.07
Smoking	149 (16.9)	0.45	< 0.05
Test for chest pain reason	501 (56.7)	< 0.05	< 0.05
Test for equivocal reason	66 (7.5)	0.09	0.81
Dyspnea	547 (61.9)	0.15	< 0.05
Palpitations	414 (46.8)	< 0.05	0.44
Syncope	280 (31.7)	0.18	0.83
Aspirin	514 (58.1)	< 0.05	< 0.05
ACE inhibitors	240 (27.1)	< 0.05	< 0.05
Beta-blockers	390 (44.1)	< 0.05	< 0.05
Calcium Channel Blockers	132 (14.9)	0.24	< 0.05
Diuretics	157 (17.8)	0.57	0.06
Statins	458 (51.8)	0.10	0.07

CAD, coronary artery disease; SD, standard deviation; HR, heart rate; BP, blood pressure; ACE, angiotensin-converting enzyme

best discrimination and calibration capabilities among the evaluated models in the CAD risk prediction task. It also achieved optimal performance in predicting the downstream diagnostic tests.

Regarding the selection of MLP and decoder within the TabPerceiver architecture, the decoder performed marginally better when used as the output layer.

### C. Feature Importance

Fig. 7 shows the results of the ablation study. It demonstrates that segment readings such as stenosis and calcification degrees have a stronger impact on model performance than other feature modalities, such as demographical characteristics and other tests received by the patient. Multi-tasking Tabperceiver achieved the optimized performance on the selected features from different feature modalities. Feature ranking obtained using SHAP turned out to be the most effective guide for feature selection in both GBDT and deep learning models for CAD risk and down-streaming test prediction. Fig. 8 shows the feature importance ranking by their SHAP values in the GBDT model. Clinical information such as blood pressure and heart rate are revealed to be important predictors for both tasks, as well as the Agatston score which relate to the result and the confidence in the interpretation of the CCTA test. Similar to the previous studies, age and hypertension were found to be significant risk factors for CAD [4], [35]. CCTA segment readings and pre-test probability also had an important role in predicting both tasks. This was also consistent with the results of the ablation study.

## IV. DISCUSSION

Coronary artery disease is a commonly encountered disease associated with significant morbidity, mortality, and high medical costs.

TABLE II  
PERFORMANCE COMPARISON AMONG DIFFERENT MACHINE LEARNING METHODS

Models	Target	Performance			
		AUC (95% CI)	Sensitivity	Specificity	Brier Score
GBDT	low	0.733 (0.721, 0.747)	0.58	0.83	0.31
	medium	0.602 (0.589, 0.616)	0.18	0.81	0.25
	high	0.719 (0.706, 0.732)	0.68	0.63	0.34
	invasive test	0.730 (0.715, 0.745)	0.64	0.42	0.34
MLP	low	0.685 (0.665, 0.705)	0.51	0.82	0.32
	medium	0.593 (0.577, 0.609)	0.19	0.80	0.29
	high	0.696 (0.676, 0.716)	0.65	0.57	0.35
	invasive test	0.694 (0.681, 0.706)	0.70	0.71	0.33
TabPerceiver (MLP)	low	0.723 (0.711, 0.734)	0.54	0.83	0.31
	medium	0.602 (0.590, 0.615)	0.19	0.80	0.27
	high	0.713 (0.702, 0.725)	0.68	0.63	0.34
	invasive test	0.704 (0.693, 0.681)	0.69	0.41	0.33
TabPerceiver (decoder)	low	0.717 (0.705, 0.729)	0.53	0.83	0.30
	medium	0.588 (0.574, 0.601)	0.17	0.80	0.27
	high	0.703 (0.690, 0.715)	0.68	0.62	0.36
	invasive test	0.688 (0.677, 0.699)	0.72	0.42	0.33
ML-TabPerceiver (MLP)	low	0.723 (0.711, 0.734)	0.54	0.83	0.31
	medium	0.602 (0.590, 0.615)	0.19	0.80	0.27
	high	0.713 (0.702, 0.725)	0.68	0.63	0.34
	invasive test	0.704 (0.693, 0.681)	0.69	0.41	0.33
ML-TabPerceiver (decoder)	low	<b>0.752</b> (0.742, 0.763)	0.59	0.85	0.29
	medium	<b>0.625</b> (0.611, 0.640)	0.22	0.81	0.27
	high	<b>0.754</b> (0.744, 0.764)	0.70	0.66	0.31
	invasive test	0.723 (0.711, 0.735)	0.71	0.44	0.32

GBDT, gradient boosting decision tree; MLP, multi-layer perceptron; ML, multi-task learning; AUC, area under the receiver operating characteristic curve; CI, confidence interval

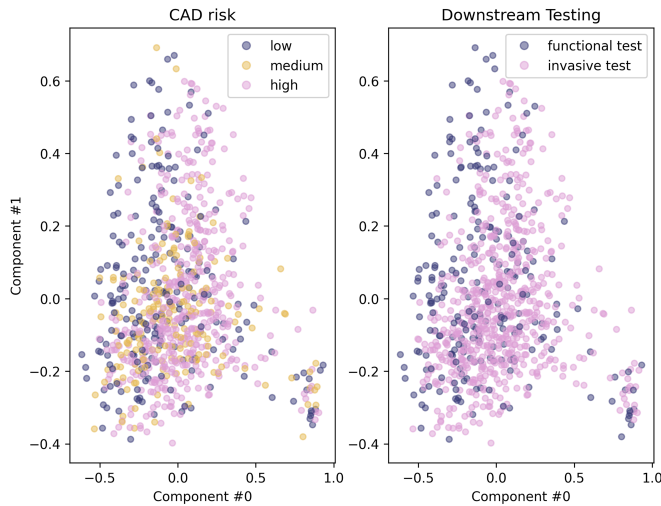


Fig. 6. Task profile. CAD risk and down-streaming tests are visualized separately using kernalized Principal Component Analysis with 2 principal components. Classes are separated by colors. Each point is a patient entry.

It has been common in clinical practice to deploy a validated pretest probability model for CAD to guide the diagnostic test selection. The majority of existing tools primarily focus on the selection of gate-keeper tests, whereas only a handful of systems contain information on downstream testing or treatment [8], [9]. Hence, there is a need for models that are based on clinical observations, which can predict the need for downstream tests or treatments in order to identify patients who are at high risk and would benefit from invasive diagnostic tests or revascularization. This study used patient clinical characteristics and CCTA segment readings to predict the risk of CAD and selection of downstream tests or treatments. We employed a transformer-based tabular deep learning model as a novel optimized analytical approach

to create clinical decision support models. Our results show that the developed multi-task TabPerceiver model is effective in predicting the risk of CAD and the selection of downstream tests or treatments. Additionally, we found that the model has appropriate calibration (the predicted probabilities of outcome reflect true probabilities of the outcome).

The use of the ML model in a clinical setting could streamline the identification of patients who may benefit from invasive diagnostic evaluation and revascularization, reducing the need for time-consuming routine clinical steps. Meanwhile, the overuse of diagnostic imaging modalities is a major issue causing significant stress on the health budget [10], [36]. To address this, there has been an increased focus on the application of risk stratification and pre-test probability assessment prior to initiation of downstream testing [5], [11]. Despite this, multiple studies have demonstrated that these risk assessment models performed sub-optimally in certain cohorts [37], [38]. In recent years, various models have been validated in multiple external populations, with a trend towards a decline in discriminative capacity [4], [39]. Indeed, differences in derivation (utilization of various imaging modalities as well as different cut-off values for the definition of CAD risk, adoption of various data processing methodologies), model complexity and inconsistent external validation limit their usefulness in clinical practice. In an ever-changing environment where populations are longitudinally evolving due to changes in dietary habits, environmental exposures, advances in science and technology, it is essential to have models that adapt over time. To address this need, machine learning has been increasingly used in the cardiovascular field. Machine learning involves algorithms that are specifically designed to identify relationships between data that go beyond the traditional linear statistical approaches.

Moreover, machine learning leverages the growing accessibility of computational power and storage space to rapidly produce meaningful results based on complex input data. Furthermore, machine learning has proven itself to be a powerful tool for diagnosing coronary artery disease [40]. We further demonstrate the robustness of TabPerceiver

on noisy data, in comparison to the baseline MLP. We evaluated these two scenarios on categorical and continuous features to specifically demonstrate the robustness of contextual embeddings from the Perceiver encoder layers.

In our multitask learning framework, the Perceiver encoder was devised to represent task-specific features. The model with common-task neurons, which comprised approximately 20% of the perceiver layer, achieved the best performance. The introduction of common-task layers into the perceiver layer can assist in learning the shared complementary information for different tasks. These findings demonstrate that multitask learning can enhance the prediction performance of the correlated tasks. Additionally, it has the advantage of improving data efficiency and reducing over-fitting through shared representations. This can be attributed to the fact that prediction with the associated task can reduce model overfitting and the impact of noisy information from the heterogeneous tumor by learning related and complementary features.

The deep feature/prediction from multiple tasks in the TabPerceiver was fused using three information fusion strategies. The results indicate the effectiveness of the methods compared to the GBDT. The experimental results show the superior performance of our multitask-learning-based model over single-task learning.

Feature concatenation may enhance the combination of complementary features while also replicating information from various sources of categorical and continuous features.

The limited sample size and input seem to hinder the predictive performance of all the models for patients with moderate (medium) risk of CAD. This is consistent with prior findings that current information remains limited for clinicians to accurately determine risk for patients in intermediate risk ranges [41]. In the risk prediction task, we chose the class with the highest probability. Hence, the sensitivity of predicting low and moderate risk was low as expected, since the low prevalence of events has affected the sensitivity and specificity.

It is important to note that validating the proposed model with tuned hyper-parameters on an additional dataset is of vital importance for the generalization and clinical applications of the model. However, medical imaging tabular data from different datasets/cohorts are usually distinct from each other. This may induce bias and inconsistent results for the tabular data-based model. It would be valuable to conduct further research to assess our design strategy when a large dataset becomes available in the future.

In our single task learning experiment, the deep models performed poorly on small tabular datasets and were no better than GBDT. We proposed the use of multi-task TabPerceiver using feature embed-

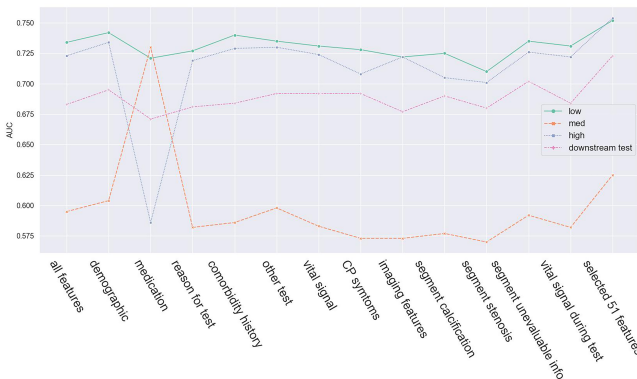


Fig. 7. Ablation study with exclusion of different feature modalities by CAD risk group and downstream tests. CAD, coronary artery disease, CP, chest pain, info., information.

TABLE III

IMPACT OF FEATURE SELECTION ON MODEL PERFORMANCE

Models	Number of input features	Target	AUC (95% CI)
GBDT	146	low	0.733 (0.721, 0.747)
		medium	0.602 (0.589, 0.616)
		high	0.719 (0.706, 0.732)
		invasive test	0.730 (0.715, 0.745)
	51	low	0.726 (0.712, 0.740)
		medium	0.610 (0.595, 0.626)
		high	0.715 (0.701, 0.729)
		invasive test	0.741 (0.731, 0.752)
MLP	146	low	0.660 (0.649, 0.672)
		medium	0.580 (0.571, 0.590)
		high	0.672 (0.661, 0.684)
		invasive test	0.669 (0.656, 0.682)
	51	low	0.685 (0.665, 0.705)
		medium	0.593 (0.577, 0.609)
		high	0.696 (0.676, 0.716)
		invasive test	0.694 (0.681, 0.706)
TabPerceiver	146	low	0.689 (0.671, 0.702)
		medium	0.573 (0.556, 0.592)
		high	0.631 (0.605, 0.658)
		invasive test	0.680 (0.669, 0.692)
	51	low	0.700 (0.687, 0.712)
		medium	0.593 (0.585, 0.607)
		high	0.673 (0.663, 0.682)
		invasive test	0.685 (0.676, 0.704)
ML-TabPerceiver	146	low	0.734 (0.724, 0.745)
		medium	0.595 (0.579, 0.610)
		high	0.723 (0.711, 0.735)
		invasive test	0.683 (0.664, 0.702)
	51	low	0.752 (0.742, 0.763)
		medium	0.629 (0.616, 0.643)
		high	0.756 (0.746, 0.767)
		invasive test	0.730 (0.715, 0.745)

GBDT, gradient boosting decision tree; MLP, multi-layer perceptron; ML, multi-task learning; AUC, area under the receiver operating characteristic curve; CI, confidence interval

dings and an attention-based module. This architecture performed better than the single-task deep learning model we experimented with. We also examined the trade offs between various architecture, computational inference cost, and hyper-parameter optimization time, which are important in real-world applications. Our analysis demonstrates that the deep learning models are more sensitive to input features. As showed in Table. III, the prediction accuracy of GBDT is not significantly impacted by feature selection, however, removing uninformative features has improved the performance of deep learning models. This has also reported in the recent study [42]. Additionally, it is much more challenging to optimize deep models than GBDT on a new dataset, due to their large number of hyper-parameters and high computational cost. However, we discovered that TabPerceiver performed effectively on tabular data while incurring a lower computational burden.

Follow-up admission and mortality outcome information for the entire cohort is not available in our dataset. We have thus used test readings and interpretation to define the risk of CAD for patients, resulting in a significant reduction in the sample size of the study cohort. This may introduce potential bias to our study and limit the performance of our GBDT and deep learning models, as it has been found to be tailored towards big data. Future validation might be required using a large cohort. The transformer-based model has showed its effectiveness in handling images, audio and text data. The perceiver architecture is also designed to process large input and output. In future work, we would like to incorporate both tabular and imaging data into the model, where further performance enhancement

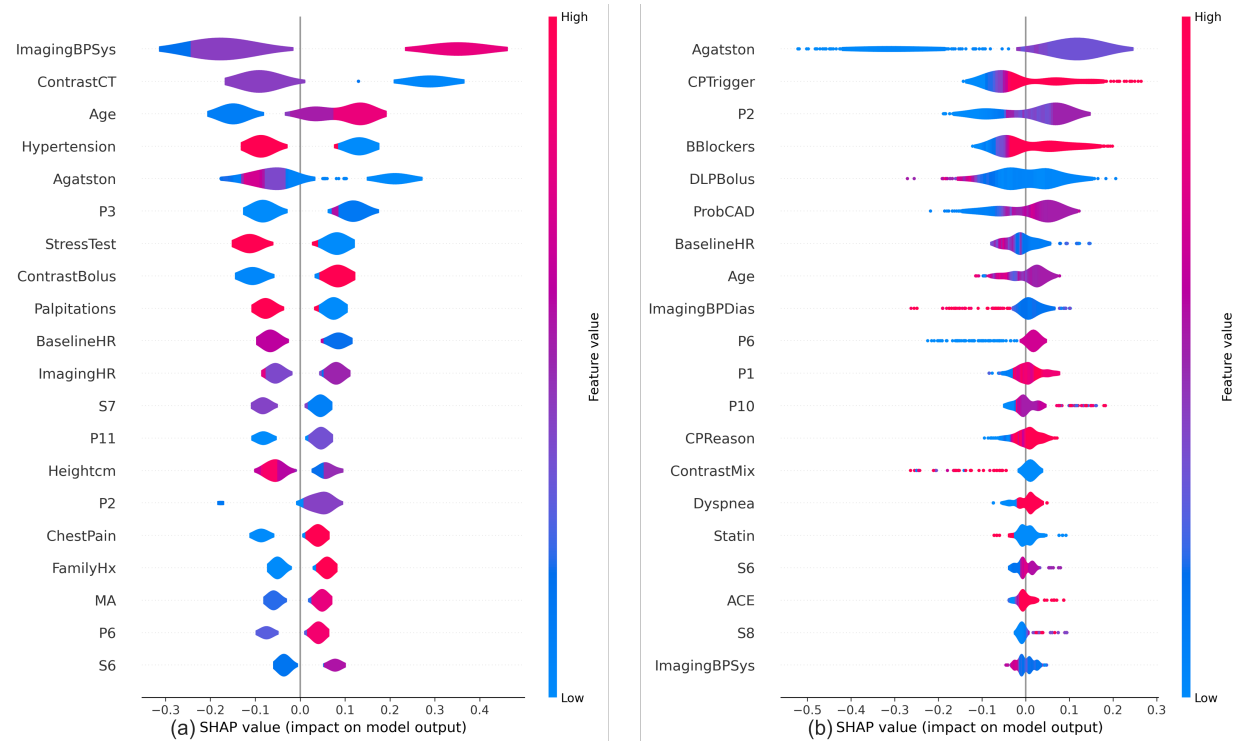


**Fig. 8.** Feature importance for predicting risk of CAD (a) and down-streaming diagnostic test (b). Blood pressure, age, hypertension and segment readings are ranked as the top important features for predicting patients' risk of CAD. Agatston score is the most determinative feature for down-streaming test selection. Other important features include blood pressure, segment readings, beta-blocker and chest pain trigger. CT, computed tomography, HR, heart rate, FamilyHx, family history, P3, calcified level of distal right coronary, S7, stenosis level of mid left anterior descending artery, P11, calcified level of proximal left circumflex artery, P2, calcified level of mid right coronary artery, MA, milliampere-seconds, P6, calcified level of proximal left anterior descending artery, S6, stenosis level of proximal left anterior descending artery, CP, chest pain; DLP, dose length product; P2, calcified level of mid right coronary artery; ProbCAD, pre-test probability of CAD (Diamond & Forrester); BPDias, diastolic blood pressure; P1, calcified level of proximal right coronary artery; P10, calcified level of the second diagonal artery; ACE, angiotensin converting enzyme inhibitors; S8, stenosis level of distal left anterior descending artery; BPSys, systolic blood pressure

may be expected.

## V. CONCLUSION AND FUTURE WORK

We propose TabPerceiver, a novel deep learning tabular data modeling architecture, that is easy to use and computationally efficient. Our deep learning model outperforms MLP in single task learning, and the performance of multi-tasking TabPerceiver was comparable to or better than that of the GBDT. It appears that deep learning tabular architectures benefit from multi-task learning. We have also demonstrated that feature selection is an essential step for deep learning tabular data modeling. Together with proper feature embedding (both categorical and continuous feature embedding), these strategies address the drawbacks of deep learning on tabular data. In a future study, we plan to incorporate more data modalities, such as actual CTA images and clinical text reports, into the model to improve the prediction of risk of CAD and support the selection of downstream diagnostic testing and treatments.

## VI. APPENDIX

Table IV: Candidate and selected features

Feature modality	Feature	Type	Select
	Age (year)	cont.	yes

Table IV: Candidate and selected features (Continued)

Feature modality	Feature	Type	Select
	Male	binary	no
	Height (cm)	cont.	no
	Weight (kg)	cont.	yes
	Smoking	CAT	yes
	Probability of CAD	cont.	yes
Vital sign	Baseline HR (bpm)	cont.	yes
	Baseline Systolic BP (mmHg)	cont.	no
	Baseline Diastolic BP (mmHg)	cont.	no
Vital sign (imaging)	Imaging HR (bpm)	cont.	yes
	Imaging Systolic BP (mmHg)	cont.	yes
	Imaging Diastolic BP (mmHg)	cont.	no
Reason for test	Ventricular tachycardia reason	binary	no
	Chest pain reason	binary	yes
	Equivocal reason	binary	no
	Rule out CAD reason	binary	yes
	Dyspnea reason	binary	no
	CHF reason	binary	no
Other tests	Stress test	binary	no
	Stress Echo	binary	no
	RNA	binary	yes
	Myocardial perfusion imaging	binary	yes
	Myocardial viability	binary	yes



Table IV: Candidate and selected features (Continued)

Feature modality	Feature	Type	Select
Medications	ACE inhibitors	binary	no
	Aspirin	binary	yes
	AT2	binary	no
	Beta blockers	binary	yes
	Calcium channel blockers	binary	no
	Insulin	binary	no
	Metformin	binary	no
	NOACs	binary	no
	Statins	binary	no
	Diuretics	binary	no
	Ticlopidine	binary	no
	PPI	binary	no
	Nitrates	binary	no
	Other oral hypoglycemics	binary	no
	Vasodilators	binary	yes
Warfarin	binary	no	
Comorbidity and other history	Valvular heart disease	binary	no
	Valvular repair or replacement	binary	no
	Congenital heart disease	binary	no
	Dyspnea	binary	no
	Hypertension	binary	yes
	Congestive heart failure	binary	no
	Palpitations	binary	yes
	Cardiac implants	binary	no
	Renal insufficiency	binary	yes
	Hyperlipidemia	binary	no
	Prior CABG	binary	yes
	Prior Catheterisation	binary	yes
	Myocardial infarction	binary	yes
	CAD	binary	no
	Diabetes mellitus	binary	no
Family history	binary	yes	
PVD	binary	no	
Syncope	binary	no	
RP	binary	yes	
CD	binary	no	
	Proximal right coronary artery calcified level (P1)	CAT	no
	stenosis level (S1)	CAT	yes
	Mid right coronary artery calcified level (P2)	CAT	yes
	stenosis level (S2)	CAT	no
	Distal right coronary artery calcified level (P3)	CAT	no
	stenosis level (S3)	CAT	yes
	Posterior interventricular artery calcified level (P4)	CAT	no
	stenosis level (S4)	CAT	no
	Left main calcified level (P5)	CAT	yes
	stenosis level (S5)	CAT	no
	Proximal left anterior descending artery calcified level (P6)	CAT	yes
	stenosis level (S6)	CAT	yes
	Mid left anterior descending artery calcified level (P7)	CAT	yes

Continued on next page

Table IV: Candidate and selected features (Continued)

Feature modality	Feature	Type	Select
	stenosis level (S7)	CAT	yes
	Distal left anterior descending artery calcified level (P8)	CAT	yes
	stenosis level (S8)	CAT	yes
	The first diagonal artery (D1) calcified level (P9)	CAT	yes
	stenosis level (S9)	CAT	yes
	The second diagonal artery (D2) calcified level (P10)	CAT	no
	stenosis level (S10)	CAT	yes
	Proximal left circumflex artery calcified level (P11)	CAT	yes
	stenosis level (S11)	CAT	yes
	The first marginal artery (M1) calcified level (P12)	CAT	no
	stenosis level (S12)	CAT	yes
	Mid left circumflex artery calcified level (P13)	CAT	no
	stenosis level (S13)	CAT	no
	The second marginal artery (M2) calcified level (P14)	CAT	yes
	stenosis level (S14)	CAT	no
Distal left circumflex artery calcified level (P15)	CAT	no	
stenosis level (S15)	CAT	no	
Left ventricle calcified level (P16)	CAT	no	
stenosis level (S16)	CAT	no	
Ramus intermedius calcified level (P17)	CAT	no	
stenosis level (S17)	CAT	yes	
Other segments calcified level (P18-22)	CAT	no	
stenosis level (S18-22)	CAT	no	
unevaluable (Uneval1-22)	binary	no	
Chest pain symptoms	Chest pain trigger	binary	yes
	Chest pain relieved	binary	no
	Chest pain	binary	yes
	Dominance	CAT	no
	Agatston	cont.	yes
	Contrast Bolus	cont.	no
	Contrast CT	cont.	yes
	Contrast Mix	cont.	no
	Contrast Mix Percent	cont.	no
	Contrast Mix Rate	cont.	no
	Contrast Type	CAT	no
	DLP Bolus	cont.	yes
	DLP Cardiac	cont.	yes
	DLP non contrast	cont.	no
	Left ventricular end-diastolic volume	cont.	yes
Left ventricular ejection fraction	cont.	no	
Left ventricular end-systolic volume	cont.	no	
MA	cont.	yes	

Continued on next page

Table IV: Candidate and selected features (Continued)

Feature modality	Feature	Type	Select
	kV	cont.	yes
	Primary First	binary	yes

CAD, coronary artery disease; HR, heart rate; CHF, congestive heart failure; BP, blood pressure; ACE, angiotensin-converting enzyme; ASA, acetylsalicylic acid; AT2, angiotensin II type 2 receptors; NOACs, novel oral Anticoagulants; PPI, proton pump inhibitors; CABG, coronary artery bypass graft surgery; Cath, catheterization; PVD, peripheral vascular disease; RP, renal protection; CD, conduct disorder; CT, computed tomography; DLP, dose length product; MA, milliamperes-seconds; kV, X-Ray tube voltage

Table V: Model hyper-parameter

Model	Hyper-parameters
ML-TabPerceiver (selected 51 features)	batch_size=16
	num_layers=2
	input_embed_dim=128
	num_cross_attention_heads=4
	num_self_attention_layers_per_block= 4
	num_latents=8
	num_latent_channels=32
ML-TabPerceiver (all features)	bins_count=150
	weight_decay=0.01
	dropout=0
	label_smoothing=0.3
	batch_size=32
	num_layers=2
	input_embed_dim=128
ML-TabPerceiver (all features)	num_cross_attention_heads=8
	num_self_attention_layers_per_block= 2
	num_latents=16
	num_latent_channels=64
	bins_count=50
	weight_decay=0.01
	dropout=0
	label_smoothing=0.3

## REFERENCES

- [1] U. Ralapanawa and R. Sivakanesan, "Epidemiology and the Magnitude of Coronary Artery Disease and Acute Coronary Syndrome: A Narrative Review," *Journal of Epidemiology and Global Health*, vol. 11, no. 2, pp. 169–177, Jun. 2021.
- [2] S. L. James *et al.*, "Global, regional, and national incidence, prevalence, and years lived with disability for 354 diseases and injuries for 195 countries and territories, 1990–2017: a systematic analysis for the Global Burden of Disease Study 2017," *The Lancet*, vol. 392, no. 10159, pp. 1789–1858, Nov. 2018, publisher: Elsevier. [Online]. Available: [https://www.thelancet.com/journals/lancet/article/PIIS0140-6736\(18\)32279-7/fulltext](https://www.thelancet.com/journals/lancet/article/PIIS0140-6736(18)32279-7/fulltext)
- [3] F. Savira, B. H. Wang, A. R. Kompa, Z. Ademi, A. J. Owen, D. Liew, and E. Zomer, "The impact of coronary heart disease prevention on work productivity: a 10-year analysis," *European Journal of Preventive Cardiology*, vol. 28, no. 4, pp. 418–425, May 2021.
- [4] Al'Aref *et al.*, "Machine learning of clinical variables and coronary artery calcium scoring for the prediction of obstructive coronary artery disease on coronary computed tomography angiography: analysis from the CONFIRM registry," *European Heart Journal*, vol. 41, no. 3, pp. 359–367, Jan. 2020. [Online]. Available: <https://doi.org/10.1093/eurheartj/ehz565>
- [5] Task Force Members, G. Montalescot *et al.*, "2013 ESC guidelines on the management of stable coronary artery disease: The Task Force on the management of stable coronary artery disease of the European Society of Cardiology," *European Heart Journal*, vol. 34, no. 38, pp. 2949–3003, Oct. 2013. [Online]. Available: <https://doi.org/10.1093/eurheartj/ehz296>
- [6] P. S. Douglas, U. Hoffmann, M. R. Patel, D. B. Mark, H. R. Al-Khalidi, B. Cavanaugh, J. Cole, R. J. Dolor, C. B. Fordyce, M. Huang, M. A. Khan, A. S. Kosinski, M. W. Krucoff, V. Malhotra, M. H. Picard, J. E. Udelson, E. J. Velazquez, E. Yow, L. S. Cooper, and K. L. Lee, "Outcomes of Anatomical versus Functional Testing for Coronary Artery Disease," *New England Journal of Medicine*, vol. 372, no. 14, pp. 1291–1300, Apr. 2015, publisher: Massachusetts Medical Society \_eprint: <https://doi.org/10.1056/NEJMoa1415516>. [Online]. Available: <https://doi.org/10.1056/NEJMoa1415516>
- [7] A. R. van Rosendaal, A. C. Dimitriu-Leen, M. A. de Graaf, E. W. van Zwet, J. W. Jukema, J. J. Bax, L. J. Kroft, and A. J. Scholte, "Impact of computed tomography myocardial perfusion following computed tomography coronary angiography on downstream referral for invasive coronary angiography, revascularization and, outcome at 12 months," *European Heart Journal - Cardiovascular Imaging*, vol. 18, no. 9, pp. 969–977, Sep. 2017. [Online]. Available: <https://doi.org/10.1093/ehjci/jex055>
- [8] G. Morgan-Hughes, M. C. Williams, M. Loudon, C. A. Roobottom, A. Veitch, R. Van Lingen, B. Holloway, N. Bellenger, M. Schmitt, and R. Bull, "Downstream testing after CT coronary angiography: time for a rethink?" *Open Heart*, vol. 8, no. 1, 2021, publisher: Archives of Disease in childhood \_eprint: <https://openheart.bmj.com/content/8/1/e001597.full.pdf>. [Online]. Available: <https://openheart.bmj.com/content/8/1/e001597>
- [9] S. Fyyaz, J. Hudson, O. Olabintan, A. Katsigris, S. David, S. Plein, and K. Alfakih, "Computed tomography coronary angiography: Diagnostic yield and downstream testing," *Clinical Medicine*, vol. 20, no. 1, pp. 81–85, Jan. 2020. [Online]. Available: <https://www.ncbi.nlm.nih.gov/pmc/articles/PMC6964184/>
- [10] X. Huang and M. B. Rosenthal, "Overuse of Cardiovascular Services," *Circulation*, vol. 132, no. 3, pp. 205–214, Jul. 2015, publisher: American Heart Association. [Online]. Available: <https://www.ahajournals.org/doi/full/10.1161/CIRCULATIONAHA.114.-012668>
- [11] S. D. Fihn, J. C. Blankenship, K. P. Alexander, J. A. Bittl, J. G. Byrne, B. J. Fletcher, G. C. Fonarow, R. A. Lange, G. N. Levine, T. M. Maddox, S. S. Naidu, E. M. Ohman, and P. K. Smith, "2014 ACC/AHA/AATS/PCNA/SCAI/STS Focused Update of the Guideline for the Diagnosis and Management of Patients With Stable Ischemic Heart Disease," *Circulation*, vol. 130, no. 19, pp. 1749–1767, Nov. 2014, publisher: American Heart Association. [Online]. Available: <https://www.ahajournals.org/doi/full/10.1161/CIR.0000000000000095>
- [12] A. Dosovitskiy, L. Beyer, A. Kolesnikov, D. Weissenborn, X. Zhai, T. Unterthiner, M. Dehghani, M. Minderer, G. Heigold, S. Gelly, J. Uszkoreit, and N. Houlsby, "An Image is Worth 16x16 Words: Transformers for Image Recognition at Scale," Jun. 2021, arXiv:2010.11929 [cs]. [Online]. Available: <http://arxiv.org/abs/2010.11929>
- [13] T. B. Brown, B. Mann, N. Ryder, M. Subbiah, J. Kaplan, P. Dhariwal, A. Neelakantan, P. Shyam, G. Sastry, A. Askell, S. Agarwal, A. Herbert-Voss, G. Krueger, T. Henighan, R. Child, A. Ramesh, D. M. Ziegler, J. Wu, C. Winter, C. Hesse, M. Chen, E. Sigler, M. Litwin, S. Gray, B. Chess, J. Clark, C. Berner, S. McCandlish, A. Radford, I. Sutskever, and D. Amodei, "Language Models are Few-Shot Learners," Jul. 2020, arXiv:2005.14165 [cs]. [Online]. Available: <http://arxiv.org/abs/2005.14165>
- [14] R. Shwartz-Ziv and A. Armon, "Tabular Data: Deep Learning is Not All You Need," arXiv:2106.03253 [cs], Jun. 2021, arXiv: 2106.03253. [Online]. Available: <http://arxiv.org/abs/2106.03253>
- [15] J. Schmidhuber, "Deep learning in neural networks: an overview," *Neural Networks: The Official Journal of the International Neural Network Society*, vol. 61, pp. 85–117, Jan. 2015.
- [16] V. Borisov, T. Leemann, K. Seßler, J. Haug, M. Pawelczyk, and G. Kasneci, "Deep Neural Networks and Tabular Data: A Survey," arXiv:2110.01889 [cs], Feb. 2022, arXiv: 2110.01889. [Online]. Available: <http://arxiv.org/abs/2110.01889>
- [17] J. Tanha, M. van Someren, and H. Afsarmanesh, "Semi-supervised self-training for decision tree classifiers," *International Journal of Machine Learning and Cybernetics*, vol. 8, no. 1, pp. 355–370, Feb. 2017. [Online]. Available: <https://doi.org/10.1007/s13042-015-0328-7>
- [18] J. Devlin, M.-W. Chang, K. Lee, and K. Toutanova, "BERT: Pre-training of Deep Bidirectional Transformers for Language Understanding," in

- Proceedings of the 2019 Conference of the North American Chapter of the Association for Computational Linguistics: Human Language Technologies, Volume 1 (Long and Short Papers)*. Minneapolis, Minnesota: Association for Computational Linguistics, Jun. 2019, pp. 4171–4186. [Online]. Available: <https://aclanthology.org/N19-1423>
- [19] P. Xu, X. Zhu, and D. A. Clifton, “Multimodal Learning with Transformers: A Survey,” Jun. 2022, arXiv:2206.06488 [cs]. [Online]. Available: <http://arxiv.org/abs/2206.06488>
- [20] R. Caruana, “Multitask Learning,” *Machine Learning*, vol. 28, no. 1, pp. 41–75, Jul. 1997. [Online]. Available: <https://doi.org/10.1023/A:1007379606734>
- [21] Y. Zhang and Q. Yang, “An overview of multi-task learning,” *National Science Review*, vol. 5, no. 1, pp. 30–43, Jan. 2018. [Online]. Available: <https://doi.org/10.1093/nsr/nwx105>
- [22] G. A. Diamond and J. S. Forrester, “Analysis of probability as an aid in the clinical diagnosis of coronary-artery disease,” *The New England Journal of Medicine*, vol. 300, no. 24, pp. 1350–1358, Jun. 1979.
- [23] S. v. Buuren and K. Groothuis-Oudshoorn, “mice: Multivariate Imputation by Chained Equations in R,” *Journal of Statistical Software*, vol. 45, pp. 1–67, Dec. 2011. [Online]. Available: <https://doi.org/10.18637/jss.v045.i03>
- [24] M. Czaja, Z. Wygoda, A. Duszańska, D. Szczerba, J. Głowacki, M. Gašior, and J. P. Wasilewski, “Interpreting myocardial perfusion scintigraphy using single-photon emission computed tomography. part 1,” *Kardiologia i Torakochirurgia Polska/Polish Journal of Thoracic and Cardiovascular Surgery*, vol. 14, no. 3, pp. 192–199, 2017.
- [25] A. Jaegle, S. Borgeaud, J.-B. Alayrac, C. Doersch, C. Ionescu, D. Ding, S. Koppula, D. Zoran, A. Brock, E. Shelhamer, O. Hénaff, M. M. Botvinick, A. Zisserman, O. Vinyals, and J. Carreira, “Perceiver IO: A General Architecture for Structured Inputs & Outputs,” Mar. 2022, arXiv:2107.14795 [cs, eess]. [Online]. Available: <http://arxiv.org/abs/2107.14795>
- [26] X. Huang, A. Khetan, M. Cvitkovic, and Z. Karmin, “TabTransformer: Tabular Data Modeling Using Contextual Embeddings,” Dec. 2020, arXiv:2012.06678 [cs]. [Online]. Available: <http://arxiv.org/abs/2012.06678>
- [27] A. Jaegle, F. Gimeno, A. Brock, A. Zisserman, O. Vinyals, and J. Carreira, “Perceiver: General Perception with Iterative Attention,” arXiv:2103.03206 [cs, eess], Jun. 2021, arXiv: 2103.03206. [Online]. Available: <http://arxiv.org/abs/2103.03206>
- [28] A. Vaswani, N. Shazeer, N. Parmar, J. Uszkoreit, L. Jones, A. N. Gomez, L. Kaiser, and I. Polosukhin, “Attention Is All You Need,” Dec. 2017, arXiv:1706.03762 [cs]. [Online]. Available: <http://arxiv.org/abs/1706.03762>
- [29] A. Radford, J. Wu, R. Child, D. Luan, D. Amodei, and I. Sutskever, “Language models are unsupervised multitask learners,” *OpenAI blog*, vol. 1, no. 8, p. 9, 2019.
- [30] Y. Gorishniy, I. Rubachev, and A. Babenko, “On Embeddings for Numerical Features in Tabular Deep Learning,” Mar. 2022, arXiv:2203.05556 [cs]. [Online]. Available: <http://arxiv.org/abs/2203.05556>
- [31] S. Ruder, “An Overview of Multi-Task Learning in Deep Neural Networks,” Jun. 2017, arXiv:1706.05098 [cs, stat]. [Online]. Available: <http://arxiv.org/abs/1706.05098>
- [32] A. Kendall, Y. Gal, and R. Cipolla, “Multi-Task Learning Using Uncertainty to Weigh Losses for Scene Geometry and Semantics,” Apr. 2018, arXiv:1705.07115 [cs]. [Online]. Available: <http://arxiv.org/abs/1705.07115>
- [33] S. M. Lundberg and S.-I. Lee, “A Unified Approach to Interpreting Model Predictions,” in *Advances in Neural Information Processing Systems*, vol. 30. Curran Associates, Inc., 2017. [Online]. Available: <https://proceedings.neurips.cc/paper/2017/hash/8a20a8621978632d76c4-3dfd28b67767-Abstract.html>
- [34] B. Shariari, K. Swersky, Z. Wang, R. P. Adams, and N. de Freitas, “Taking the Human Out of the Loop: A Review of Bayesian Optimization,” *Proceedings of the IEEE*, vol. 104, no. 1, pp. 148–175, Jan. 2016, conference Name: Proceedings of the IEEE.
- [35] A. N. Nowbar, M. Gitto, J. P. Howard, D. P. Francis, and R. Al-Lamee, “Mortality From Ischemic Heart Disease,” *Circulation: Cardiovascular Quality and Outcomes*, vol. 12, no. 6, p. e005375, Jun. 2019, publisher: American Heart Association. [Online]. Available: <https://www.ahajournals.org/doi/full/10.1161/CIRCOUTCOMES.118.-005375>
- [36] J. L. J. M. Müskens, R. B. Kool, S. A. v. Dulmen, and G. P. Westert, “Overuse of diagnostic testing in healthcare: a systematic review,” *BMJ Quality & Safety*, vol. 31, no. 1, pp. 54–63, Jan. 2022, publisher: BMJ Publishing Group Ltd Section: Systematic review. [Online]. Available: <https://qualitysafety.bmj.com/content/31/1/54>
- [37] K. K. Kumamaru, T. Arai, H. Morita, T. Sekine, K. Takamura, S. Takase, F. J. Rybicki, and T. Kondo, “Overestimation of pretest probability of coronary artery disease by Duke clinical score in patients undergoing coronary CT angiography in a Japanese population,” *Journal of Cardiovascular Computed Tomography*, vol. 8, no. 3, pp. 198–204, Jun. 2014.
- [38] L. Baskaran, I. Danad, H. Gransar, B. Ó Hartaigh, J. Schulman-Marcus, F. Y. Lin, J. M. Peña, A. Hunter, D. E. Newby, P. D. Adamson, and J. K. Min, “A Comparison of the Updated Diamond-Forrester, CAD Consortium, and CONFIRM History-Based Risk Scores for Predicting Obstructive Coronary Artery Disease in Patients With Stable Chest Pain: The SCOT-HEART Coronary CTA Cohort,” *JACC: Cardiovascular Imaging*, vol. 12, no. 7, Part 2, pp. 1392–1400, Jul. 2019. [Online]. Available: <https://www.sciencedirect.com/science/article/pii/S1936878X18302213>
- [39] T. He, X. Liu, N. Xu, Y. Li, Q. Wu, M. Liu, and H. Yuan, “Diagnostic models of the pre-test probability of stable coronary artery disease: A systematic review,” *Clinics*, vol. 72, no. 3, pp. 188–196, Mar. 2017. [Online]. Available: <https://www.ncbi.nlm.nih.gov/pmc/articles/PMC5350262/>
- [40] R. Alizadehsani, M. Abdar, M. Roshanzamir, A. Khosravi, P. M. Kebria, F. Khozeimeh, S. Nahavandi, N. Sarrafzadegan, and U. R. Acharya, “Machine learning-based coronary artery disease diagnosis: A comprehensive review,” *Computers in Biology and Medicine*, vol. 111, p. 103346, Aug. 2019. [Online]. Available: <https://www.sciencedirect.com/science/article/pii/S001048251930215X>
- [41] R. C. Pasternak, J. Abrams, P. Greenland, L. A. Smaha, P. W. F. Wilson, and M. N. Houston, “Task force #1—identification of coronary heart disease risk: is there a detection gap?” *Journal of the American College of Cardiology*, vol. 41, no. 11, pp. 1863–1874, Jun. 2003, publisher: American College of Cardiology Foundation. [Online]. Available: [https://www.jacc.org/doi/abs/10.1016/S0735-1097\(03\)00358-9](https://www.jacc.org/doi/abs/10.1016/S0735-1097(03)00358-9)
- [42] L. Grinsztajn, E. Oyallon, and G. Varoquaux, “Why do tree-based models still outperform deep learning on tabular data?” Jul. 2022, arXiv:2207.08815 [cs, stat]. [Online]. Available: <http://arxiv.org/abs/2207.08815>